Table 1. Mutations and non-pathogenic variants in congenital or early-onset auditory neuropathy

Types of variants	Location	Nucleotide variation	Predicted amino acid change	Allele frequency in normal controls	Novel or known
Mutations					
Missense substitution	Exon 15	c.1621G>A	p.G541S	0/376	Novel
	Exon 46	c.5524G>A	p.D1842N	0/376	Novel
	Exon 50	c.5816G>A	p.R1939Q	1/378	Known
Frameshift	Exon 17	c.1946-1965del20	p.R649PfsX5	0/192	Novel
Nonsense	Exon 14	c.1422T>A	p.Y474X	0/192	Novel
	Exon 46	c.5466C>G	p.Y1822X	0/192	Novel
Non-stop substitution	Exon 50	c.5992T>C	p.X1988RextX30	0/192	Novel
Putative splice site mutations					
	Exon 9 IVS	IVS9+5G>A		0/362	Novel
	Exon 47 IVS	IVS47-2A>G		0/190	Known
Non-pathogenic variants					
	Exon 2	c.129C>T	p.D43D	NT	Known
	Exon 3	c.145C>T	p.R49W	3/192	Known
	Exon 3	c.158C>T	p.A53V	75/192	Known
	Exon 4	c.244C>T	p.R82C	29/192	Known
	Exon 5	c.372A>G	p.T124T	NT	Known
	Exon 19	c.62C>T	p.P21L	172/172	Known
	Exon 23	c.2452C>T	p.R818W	0/188	Known
	Exon 24	c.2580C>G	p.V860V	NT	Known
	Exon 24	c.2613C>T	p.L861L	NT	Known
	Exon 25	c.2703G>A	p.S901S	NT	Known
	Exon 25	c.2736G>C	p.L912L	NT	Known
	Exon 41	c.4677G>A	p.V1559V	NT	Known
	Exon 41	c.4767C>T	p.R1589R	NT	Known
	Exon 43	c.5026C>T	p.R1676C	8/188	Known
	Exon 43	c.5091G>A	p.P1697P	NT	Novel
	Exon 45	c.5331C>T	p.D1777D	NT	Known

C2 domains, four C2 domains, and one C2 domain, respectively.

p.X1988RextX30, in which the stop codon is affected and 30 residues are added to the C terminus, accompanied p.R1939Q in a compound heterozygote (patient 12). Because the stop codon is separated by only one residue from the transmembrane domain, the additional C-terminal tail residues would interfere with anchoring to the membrane, which is critical for proper function. The three subjects with only one pathogenic *OTOF* allele (patient 14, patient 15, and patient 16) are likely to have mutations which could not be identified in the present study rather than just be coincidental carriers. Mutations which were not excluded in the present study include those in introns, a previously unknown exon, or a distant enhancer/promotor region as well as large deletions or other sequence rearrangements.

Screening of other genes revealed that one patient who did not have any mutations in *OTOF* was a compound heterozygote of *GJB2* mutations (patient 21). The AN phenotype has been reported in subjects with *GJB2* mutations (25). We identified three other patients with biallelic *OTOF* mutations that had heterozygous *GJB2* mutations, but they were considered to be coincidental. Distribution of patients carrying different pathogenic GJB2 alleles was shown in Fig. 1 (outer circle). None of the patients had A1555G or A3243G mitochondrial DNA mutations. Mutations in *PJVK* were not detected in six patients who did not have any mutations in *OTOF* or *GJB2* as well as in three patients who were heterozygous for *OTOF* mutation without mutations in *GJB2*.

All but one patient had a single haplotype associated with the p.R1939Q variant, which was not represented in 22 wild-type alleles in the parents, and representative SNPs and their allele frequencies as well as haplotypes are shown in Fig. 4a,b. Patient 2 had recombination of the same p.R1939Q-associated haplotype with the wild-type haplotype from his father. These results indicated that all the chromosomes carrying p.R1939Q were derived from a common ancestor.

Clinical findings

Clinical features of the patients are shown in Table 2. A consistent phenotype was present in seven patients carrying homozygous p.R1939Q and four patients who had heterozygous p.R1939Q accompanied by heterozygous truncating or putative splice site mutations. Patient 12, a compound heterozygote of p.R1939Q and a non-truncating mutation, showed a distinct phenoytpe. Patient 13, a homozygote of another non-truncating mutation, presented with temperature-sensitive AN.

Table 2. Genetic and clinical features of patients with congenital or early-onset auditory neuropathy

OTOF genotype[a]	Patient ID	Age, sex	*GJB2* genotype[a]	Degree of hearing loss (age of test)	Phenotype
p.R193Q/p.R1939Q					
	1	3, M	-/-	Profound (1 year 7 months)	NP, flat
	2	2, M	-/-	Profound (2 years 7 months)	NP, flat
	3	3, M	-/-	Profound (3 years 2 months)	NP, flat
	4	4, M	c.235delC/-	Profound (3 years 2 months)	NP, gently sloping
	5	2, F	-/-	profound (2 years 6 months)	NP, gently sloping
	6	2, M	-/-	Severe (2 years 10 months)	NP, flat
	7	2, M	-/-	Severe (1 year 9 months)	NP, flat
p.R1939Q/truncating or putative splice site[b]					
p.R1939Q/c.1946-1965del20	8	9, M	-/-	Unstable (2 years 10 months)	unstable, gently sloping
p.R1939Q/p.Y474X	9	2, M	-/-	Profound (1 year 7 months)	NP, flat
p.R1939Q/p.Y1822X	10	1, F	p.G45E+p.Y136X/-	Profound (2 years 0 month)	NP, flat
p.R1939Q/IVS9+5G>A	11	7, F	-/-	Profound (7 years 6 months)	NP, flat
p.R1939Q/non-truncating[c]					
p.R1939Q/p.X1988RextX30	12	29, F	p.V371/-	Moderate (29 years 1 month)	P, R: steeply sloping L: gently sloping
Non-truncating/non-truncating					
p.G541S/p.G541S	13	26, M	-/-	Mild[d] (25 years 11 months)	NP, flat
Various heterozygotes[e]					
p.R1939Q/-	14	5, F	-/-	Profound (5 years 10 months)	NP, flat
p.D1842N/-	15	2, F	-/-	Moderate (2 years 9 months)	NP, flat
IVS47-2A>G/-	16	6, F	-/-	Profound (5 years 11 months)	NP, flat
No mutations					
	17	4, F	-/-	Severe (4 years 8 months)	NP, gently sloping
	18	7, M	-/-	Profound (7 years 4 months)	NP, gently sloping
	19	6, F	-/-	Severe (5 years 7 months)	NP, R: gently sloping L: flat
	20	8, F	-/-	Profound (8 years 2 months)	NP, gently sloping
	21	3, F	p.235delC/c.176-191del16	Profound (3 years 1 month)	NP, flat
	22	7, F	-/-	Severe (7 years 10 months)	NP, flat
	23	2, M	-/-	Severe (1 year 8 months)	NP, flat

F, female; ID, identification number; M, male; NP, non-progressive; P, progressive; Phenotype (course of hearing loss and audiogram shape).
[a]No mutations.
[b]Truncating or putative splice site mutations.
[c]Non-truncating mutations.
[d]Temperature-sensitive auditory neuropathy.
[e]Mutations in heterozygotes without accompanying pathogenic mutations.

Patient 13 complained of difficulty in understanding conversation, and his hearing deteriorated when he became febrile or was exposed to loud noise according to his self-report. He explained that the deterioration varied from mild to complete loss of communication. Pure-tone audiometry when he was afebrile revealed mild hearing loss with a flat configuration. Among three patients who had only one pathogenic allele of *OTOF*, patient 15 carrying p.D1842N presented with moderate hearing loss, whereas patient 14 carrying p.R1939Q and patient 16 carrying IVS47-2A>G presented with profound hearing loss.

Discussion

The present study demonstrated biallelic *OTOF* mutations in 56.5% (13 of 23) of subjects with congenital or early-onset AN in Japanese population, indicating the most frequent cause associated with this type of AN. So far, biallelic *OTOF* mutations were identified in 22.2% (2 of 9) and 55% (11 of 20) of subjects with AN in American and Spanish studies, respectively (11, 12). In Brazilian population, 27.3% (3 of 11) of subjects with AN had *OTOF* mutations in two alleles (13). Taiwanese and Chinese subjects demonstrated that 18.2% (4 of 22)

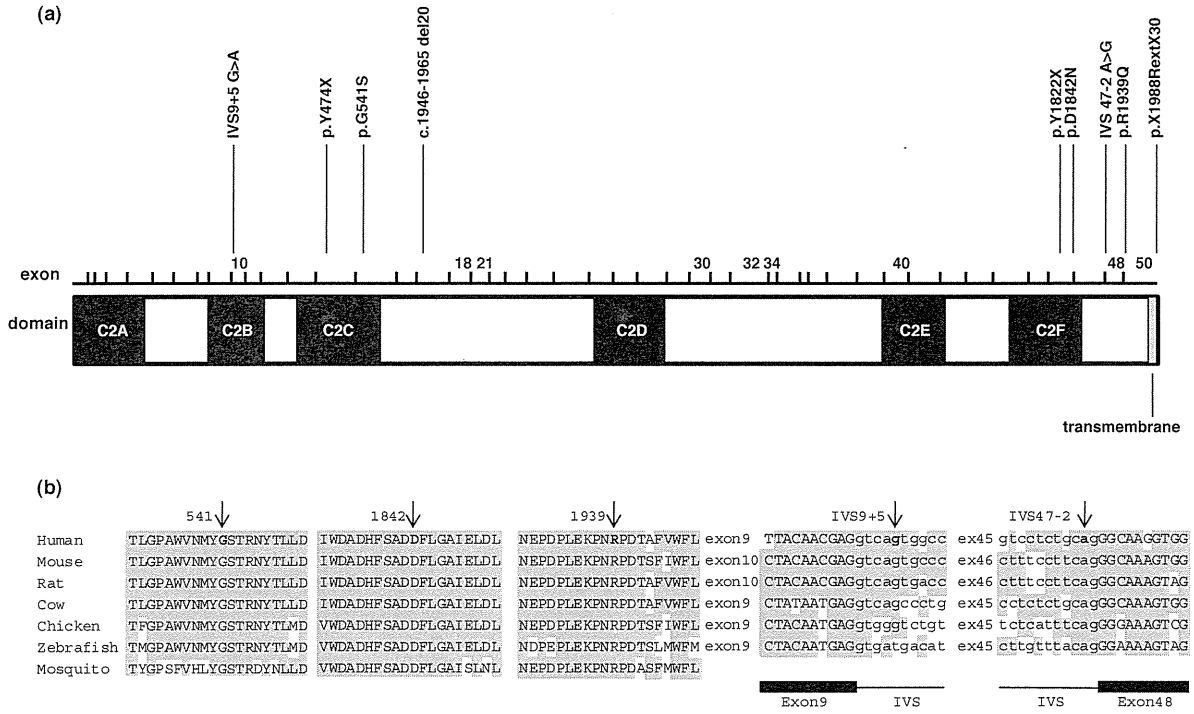

Fig. 2. The location of each mutation in *OTOF* and the evolutionary conservation of the amino acids or nucleotides affected by the missense and splice site mutations. (a) Location of mutations in the *OTOF* coding region of the cochlear isoform. Calcium-binding domains C2A through C2F are shown in black. (b) Multiple alignments of otoferlin orthologs at five non-contiguous regions and splice sites. Arrows indicate affected amino acids or nucleotides. Regions of amino acid and nucleotide sequence identity are shaded. Boundaries between introns and exons are indicated in the bottom. IVS indicates intervening sequence.

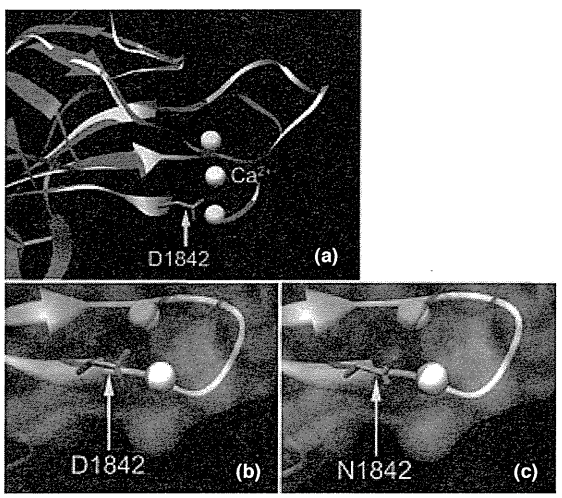

Fig. 3. Predicted three-dimensional protein structures of C2F domain in wild-type otoferlin and D1842N mutant otoferlin. (a) Ribbon model of the otoferlin C2F domain (white) superimposed onto that of the corresponding region of human protein kinase C gamma (hPKCγ, PDBID: 2UZP, chain A) which was selected as an optimal template (29.5% amino acid sequence identity) (magenta). Ca^{2+} is shown as a white sphere. The regions around D1842 of wild-type otoferlin (b) and N1842 of mutant otoferlin (c) are overlaid with their electrostatic surface potentials indicated by red (negative), blue (positive), and white (neutral). The side chains of both D1842 and N1842 are located very close (within 1.0 Å) to calcium ions. D1842N changes the electrostatic surface potential around the side chain from negative to positive in the cellular environment (pH = 7.4), and generate repulsive force on calcium ions.

and 1.4% (1 of 73), respectively, had biallelic *OTOF* mutations (14, 15).

The spectrum of *OTOF* mutations we identified differed significantly from those in other populations. Most reported *OTOF* mutations in the literature have been confined to individual families. An exception is p.Q829X, found in approximately 3% of autosomal recessive non-syndromic sensorineural hearing loss cases in the Spanish population (18). Recently, c.2905-2923delinsCTCCGAGCGCA and p.E1700Q were identified in four Argentinean families and four Taiwanese families, respectively (12, 14). In this study, p.R1939Q was detected in 13 families. Thus, p.R1939Q is now the second-most prevalent *OTOF* mutation reported. This mutation may be more common in Japan, as this mutation is found in only 1 of 10753 choromosomes in the European-American and African-American population by EVS. p.R1939Q was previously reported in one family in the United States, but the origin of the family was not detailed (19). Because no patients carrying p.R1939Q have been reported in Asian population except for the present study or in European population, this prevalent founder mutation appears to be an independent mutational event in Japanese.

Pathogenic *OTOF* mutations have been associated with stable, severe-to-profound sensorineural hearing loss with a few exceptions: c.2093+1G>T and p.P1987R were associated with stable, moderate-to-severe hearing loss (11, 19), p.E1700Q was associated with progressive, moderate-to-profound hearing

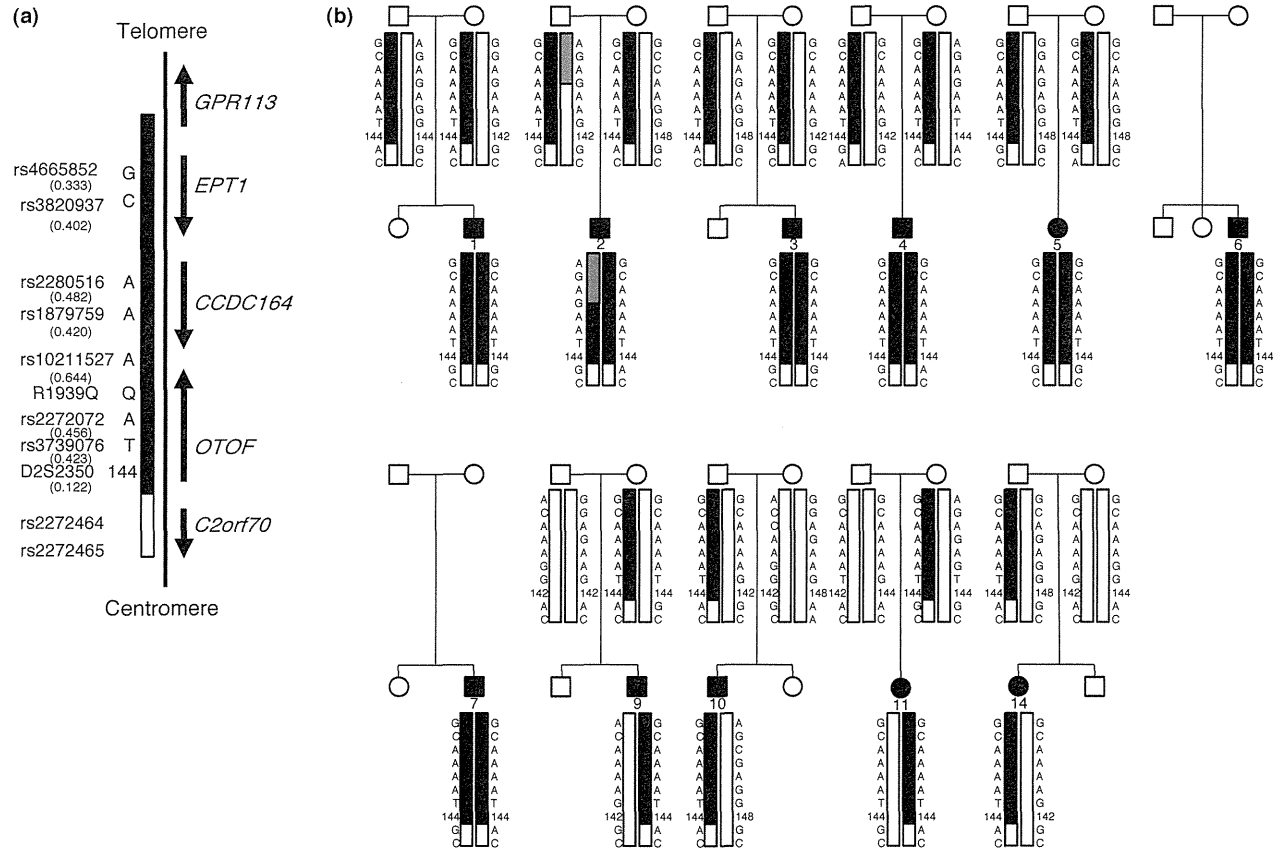

Fig. 4. Results of haplotype analysis of patients who had p.R1939Q alleles and their parents. (a) A part of tested single nucleotide polymorphisms (SNPs) and a microsatellite marker in relation to the genetic map around *OTOF* (chromosome 2p23.1). The region corresponding to the haplotype associated with the p.R1939Q mutation is indicated by black. Allele frequency of each SNP and a microsatellite marker is shown in a parenthesis. (b) Haplotypes of 11 auditory neuropathy (AN) patients with hearing loss who had p.R1939Q and their parents. The haplotype is indicated beside the vertical bars. The number under the symbol is the patient identification number in Table 2. A recombination point is indicated by grey in patient 2.

loss (14), and several mutations were associated with temperature-sensitive AN (11, 13, 15, 20). p.R1939Q homozygotes had a consistent phenotype of congenital or early-onset, stable, and severe-to-profound hearing loss with a flat or gently sloping audiogram. The same phenotype has also been reported in a family in United States, which included compound heterozygotes having p.R1939Q and a truncating mutation (19). Patients that were compound heterozygotes of p.R1939Q and truncating mutations or a putative splice site mutation also exhibited the similar phenotype in the present study. Thus, p.R1939Q variants are likely to cause severe impairment of otoferlin function. In contrast, a subject that was a compound heterozygote of p.R1939Q and a non-truncating mutation presented with a distinct phenotype of congenital or early-onset, progressive, moderate hearing loss with a steeply sloping or gently sloping audiogram. A homozygote of another non-truncating mutation also showed a distinct phenotype of temperature-sensitive AN. One of three patients who had only one allele of non-truncating mutation other than p.R1939Q presented with moderate hearing loss, whereas the other two subjects who had only one allele of p.R1939Q or a putative splice site mutation presented with profound hearing loss. These genotype–phenotype correlations of *OTOF* were similar to those of *GJB2*, i.e., more severe hearing loss was observed in subjects homozygous for truncating mutations than in subjects homozygous for non-truncating mutations, and more severe hearing loss was observed in subjects homozygous for a frameshift mutation (35delG) than in subjects compound heterozygous for the 35delG and other mutations (26, 27).

A patient with temperature-sensitive AN with a specific *OTOF* mutation was found in the present study. So far, temperature-sensitive AN has been observed in two siblings with heterozygous p.I515T without an accompanying pathogenic allele (11), three siblings with homozygous p.E1804del (20), a compound heterozygote with c.2975-2978delAG and p.R1607W (15), and a compound heterozygote with p.G614E and p.R1080P (13). The patient in this study had biallelic mutations affecting residues specific to the long isoform. Previously, two subjects showed biallelic mutations affecting this region, but they were not tested for OAE (16, 17). Thus, the present patient is the first case with biallelic mutations in this region, which indicates that mutations in the *OTOF* long isoform alone are able to cause AN.

Supporting Information

The following Supporting information is available for this article:
Table S1. Primer sequences for *OTOF*.
Table S2. Primer sequences for *PJVK*.

Additional Supporting information may be found in the online version of this article.

Please note: Wiley-Blackwell Publishing is not responsible for the content or functionality of any supplementary materials supplied by the authors. Any queries (other than missing material) should be directed to the corresponding author for the article.

Acknowledgements

We thank the families that participated in this study. We also thank Dr Yasuhide Okamoto (Inagi Municipal Hospital) and Dr Seiichi Shinden (Saiseikai Utsunomiya Hospital) for their invaluable contribution. This study was supported by a research grant of Comprehensive Research on Disability Health and Welfare from the Ministry of Health, Labor, and Welfare of Japan and a Grant-in-Aid for Clinical Research from the National Hospital Organization.

References

1. Starr A, Picton TW, Sininger Y, Hood LJ, Berlin CI. Auditory neuropathy. Brain 1996: 119: 741–753.
2. Kaga K, Nakamura M, Shinogami M, Tsuzuku T, Yamada K, Shindo M. Auditory nerve disease of both ears revealed by auditory brainstem responses, electrocochleography and otoacoustic emissions. Scand Audiol 1996: 25: 233–238.
3. Rance G, Beer DE, Cone-Wesson B et al. Clinical findings for a group of infants and young children with auditory neuropathy. Ear Hear 1999: 20: 238–252.
4. Foerst A, Beutner D, Lang-Roth R, Huttenbrink KB, von Wedel H, Walger M. Prevalence of auditory neuropathy/synaptopathy in a population of children with profound hearing loss. Int J Pediatr Otorhinolaryngol 2006: 70: 1415–1422.
5. Raveh E, Buller N, Badrana O, Attias J. Auditory neuropathy. clinical characteristics and therapeutic approach. Am J Otolaryngol 2007: 28: 302–308.
6. Yasunaga S, Grati M, Cohen-Salmon M et al. A mutation in OTOF, encoding otoferlin, a FER-1-like protein, causes DFNB9, a nonsyndromic form of deafness. Nat Genet 1999: 21: 363–369.
7. Delmaghani S, del Castillo FJ, Michel V et al. Mutations in the gene encoding pejvakin, a newly identified protein of the afferent auditory pathway, cause DFNB59 auditory neuropathy. Nat Genet 2006: 38: 770–778.
8. Schoen CJ, Emery SB, Thorne MC et al. Increased activity of Diaphanous homolog 3 (DIAPH3)/diaphanous causes hearing defects in humans with auditory neuropathy and in Drosophila. Proc Natl Acad Sci USA 2010: 107: 13396–13401.
9. Wang QJ, Li QZ, Rao SQ et al. AUNX1, a novel locus responsible for X linked recessive auditory and peripheral neuropathy, maps to Xq23-27.3. J Med Genet 2006: 43: e33.
10. Yasunaga S, Grati M, Chardenoux S et al. OTOF encodes multiple long and short isoforms: genetic evidence that the long ones underlie recessive deafness DFNB9. Am J Hum Genet 2000: 67: 591–600.
11. Varga R, Avenarius MR, Kelley PM et al. OTOF mutations revealed by genetic analysis of hearing loss families including a potential temperature sensitive auditory neuropathy allele. J Med Genet 2006: 43: 576–581.
12. Rodríguez-Ballesteros M, Reynoso R, Olarte M et al. A multicenter study on the prevalence and spectrum of mutations in the otoferlin gene (OTOF) in subjects with nonsyndromic hearing impairment and auditory neuropathy. Hum Mutat 2008: 29: 823–831.
13. Romanos J, Kimura L, Fávero ML et al. Novel OTOF mutations in Brazilian patients with auditory neuropathy. J Hum Genet 2009: 54: 382–385.
14. Chiu YH, Wu CC, Lu YC et al. Mutations in the OTOF gene in Taiwanese patients with auditory neuropathy. Audiol Neurootol 2010: 15: 364–374.
15. Wang DY, Wang YC, Weil D et al. Screening mutations of OTOF gene in Chinese patients with auditory neuropathy, including a familial case of temperature-sensitive auditory neuropathy. BMC Med Genet 2010: 26: 79.
16. Choi BY, Ahmed ZM, Riazuddin S et al. Identities and frequencies of mutations of the otoferlin gene (OTOF) causing DFNB9 deafness in Pakistan. Clin Genet 2009: 75: 237–243.
17. Mirghomizadeh F, Pfister M, Apaydin F et al. Substitutions in the conserved C2C domain of otoferlin cause DFNB9, a form of nonsyndromic autosomal recessive deafness. Neurobiol Dis 2002: 10: 157–164.
18. Rodríguez-Ballesteros M, del Castillo FJ, Martín Y et al. Auditory neuropathy in patients carrying mutations in the otoferlin gene (OTOF). Hum Mutat 2003: 22: 451–456.
19. Varga R, Kelley PM, Keats BJ et al. Non-syndromic recessive auditory neuropathy is the result of mutations in the otoferlin (OTOF) gene. J Med Genet 2003: 40: 45–50.
20. Marlin S, Feldmann D, Nguyen Y et al. Temperature-sensitive auditory neuropathy associated with an otoferlin mutation: Deafening fever!. Biochem Biophys Res Commun 2010: 394: 737–742.
21. Matsunaga T, Hirota E, Bito S, Niimi S, Usami S. Clinical course of hearing and language development in GJB2 and non-GJB2 deafness following habilitation with hearing aids. Audiol Neurootol 2006: 11: 59–68.
22. Usami S, Abe S, Akita J et al. Prevalence of mitochondrial gene mutations among hearing impaired patients. J Med Genet 2000: 37: 38–40.
23. Kiefer F, Arnold K, Künzli M, Bordoli L, Schwede T. The SWISS-MODEL Repository and associated resources. Nucleic Acid Res 2009: 37: 387–392.
24. Hilleren P, Parker R. Mechanisms of mRNA surveillance in eukaryotes. Annu Rev Genet 1999: 33: 229–260.
25. Cheng X, Li L, Brashears S et al. Connexin 26 variants and auditory neuropathy/dys-synchrony among children in schools for the deaf. Am J Med Genet A 2005: 139: 13–18.
26. Cryns K, Orzan E, Murgia A et al. Genotype-phenotypecorrelation for GJB2 (connexin 26) deafness. J Med Genet 2004: 41: 147–154.
27. Snoeckx RL, Huygen PL, Feldmann D et al. GJB2 mutations and degree of hearing loss: a multicenter study. Am J Hum Genet 2005: 77: 945–957.

Acta Oto-Laryngologica, 2012; Early Online, 1–7

informa
healthcare

ORIGINAL ARTICLE

Genetic analysis of *PAX3* for diagnosis of Waardenburg syndrome type I

TATSUO MATSUNAGA[1], HIDEKI MUTAI[1], KAZUNORI NAMBA[1], NORIKO MORITA[2] & SAWAKO MASUDA[3]

[1]*Department of Otolaryngology, Laboratory of Auditory Disorders, National Institute of Sensory Organs, National Tokyo Medical Center, Tokyo,* [2]*Department of Otolaryngology, Teikyo University School of Medicine, Tokyo and* [3]*Department of Otorhinolaryngology, Institute for Clinical Research, National Mie Hospital, Tsu, Japan*

Abstract

Conclusion: PAX3 genetic analysis increased the diagnostic accuracy for Waardenburg syndrome type I (WS1). Analysis of the three-dimensional (3D) structure of PAX3 helped verify the pathogenicity of a missense mutation, and multiple ligation-dependent probe amplification (MLPA) analysis of *PAX3* increased the sensitivity of genetic diagnosis in patients with WS1. *Objectives:* Clinical diagnosis of WS1 is often difficult in individual patients with isolated, mild, or non-specific symptoms. The objective of the present study was to facilitate the accurate diagnosis of WS1 through genetic analysis of *PAX3* and to expand the spectrum of known *PAX3* mutations. *Methods:* In two Japanese families with WS1, we conducted a clinical evaluation of symptoms and genetic analysis, which involved direct sequencing, MLPA analysis, quantitative PCR of *PAX3,* and analysis of the predicted 3D structure of PAX3. The normal-hearing control group comprised 92 subjects who had normal hearing according to pure tone audiometry. *Results:* In one family, direct sequencing of *PAX3* identified a heterozygous mutation, p. I59F. Analysis of PAX3 3D structures indicated that this mutation distorted the DNA-binding site of PAX3. In the other family, MLPA analysis and subsequent quantitative PCR detected a large, heterozygous deletion spanning 1759–2554 kb that eliminated 12–18 genes including a whole *PAX3* gene.

Keywords: *Mutation, MLPA, clinical diagnosis, hearing loss, dystopia canthorum, pigmentary disorder*

Introduction

Waardenburg syndrome (WS) is a hereditary auditory pigmentary disorder that is responsible for 1–3% of congenital deafness cases [1]. WS is classified into four types based on symptoms other than the auditory and pigmentary disorder. Type I WS (WS1) includes dystopia canthorum, and this feature distinguishes WS1 from type II WS. Type III WS is similar to WS1 but is associated with musculoskeletal anomalies of the upper limbs. Type IV WS is similar to type I but is associated with Hirschsprung disease. Diagnostic criteria for WS1 have been proposed [2]. The clinical features of WS1 demonstrate incomplete penetrance and highly varied expression [3,4], which makes diagnosis in individual patients challenging. For example, WS1 patients may present only one isolated symptom. Diagnosis of high nasal root and medial eyebrow flare can be difficult when they are mild. Hearing loss and early graying are relatively common in the general population and are not specific to WS1. Thus, the accuracy of WS1 diagnosis needs to be improved by the use of additional diagnostic procedures.

It is reported that more than 90% of patients with WS1 harbor point mutations in *PAX3* [5], and an additional 6% of WS1 patients harbor partial or complete *PAX3* deletions [6]. This high frequency of *PAX3* mutation in WS1 suggests that clinical diagnosis of WS1 could be facilitated by *PAX3* genetic analysis. To date, more than 80 *PAX3*

Correspondence: Tatsuo Matsunaga, Department of Otolaryngology, Laboratory of Auditory Disorders, National Institute of Sensory Organs, National Tokyo Medical Center, 2-5-1 Higashigaoka, Meguro, Tokyo, 152-8902, Japan. Tel: +81 3 3411 0111. Fax: +81 3 3412 9811. E-mail: matsunagatatsuo@kankakuki.go.jp

This study was presented at the annual meeting of the Collegium Oto-Rhino-Laryngologicum Amicitiae Sacrum, Rome, August 28, 2012.

(Received 19 September 2012; accepted 20 October 2012)

ISSN 0001-6489 print/ISSN 1651-2251 online
DOI: 10.3109/00016489.2012.744470

mutations are reported to be associated with WS1 [5]. A de novo paracentric inversion on chromosome 2 in a Japanese child with WS1 provided a clue for identification of *PAX3* in the distal part of chromosome 2 [7]. However, only a few *PAX3* mutations including the chromosomal inversion have been reported in Japanese patients with WS1 since then [8,9].

In the present study, we conducted *PAX3* genetic analysis to facilitate diagnosis of WS1 in two Japanese families. In one family, to verify the pathogenicity of an identified missense mutation, we analyzed the effect of the mutation on the three-dimensional (3D) structure of PAX3. In the other family, no mutations were identified by direct sequencing, so multiple ligation-dependent probe amplification (MLPA) analysis was used to search for large deletions in *PAX3* and thereby increase the sensitivity of genetic diagnosis.

Material and methods

Patients and control subjects

Two Japanese families with WS1 were included in the study. The diagnosis of WS1 was based on criteria proposed by the Waardenburg Consortium [2]. The normal-hearing controls comprised 92 subjects who had normal hearing according to pure tone audiometry. This study was approved by the institutional ethics review board at the National Tokyo Medical Center. Written informed consent was obtained from all subjects included in the study or from their parents.

Clinical evaluation

A comprehensive clinical history was taken from subjects who were examined at our hospitals or from their parents. During physical examination, special attention was given to the color of the skin, hair, and iris, and to other anomalies such as dystopia canthorum, medial eyebrow flare, limb abnormalities, and Hirschsprung disease. After otoscopic examination, behavioral audiometric testing was performed. The test protocol was selected according to the developmental age of the subject (conditioned orientation response audiometry, play audiometry, or conventional audiometric testing, from 125 to 8000 Hz), and testing was performed using a diagnostic audiometer in a soundproof room. Auditory brainstem response (ABR) and otoacoustic emission were also evaluated in some subjects.

Direct sequencing

Genomic DNA from the subjects was extracted from peripheral blood leukocytes using the Gentra Puregene® Blood kit (QIAGEN, Hamburg, Germany). Mutation screening of *PAX3* was performed by bidirectional sequencing of each exon (exons 1–11) together with the flanking intronic regions using an ABI 3730 Genetic Analyzer (Applied Biosystems, Foster City, CA, USA). Primer sequences for *PAX3* are listed in Table I. Mutation nomenclature is based on the genomic DNA sequence of [GenBank accession no. NG_011632.1], with the A of the translation initiation codon considered as +1. Nucleotide conservation between mammalian species was evaluated using ClustalW (http://www.ebi.ac.uk/Tools/msa/clustalw2/). PolyPhen-2 software (http://genetics.bwh.harvard.edu/pph2/) was used to predict the functional consequence(s) of each amino acid substitution.

MLPA

MLPA analysis was performed using an MLPA kit targeting *PAX3*, *MITF*, and *SOX10* (SALSA MLPA Kit P186-B1, MRC-Holland, Amsterdam, The Netherlands) according to the manufacturer's protocol. Exon-specific MLPA probes for exons 1–9 of *PAX3* and control probes were hybridized to genomic DNA from the subjects and normal controls and ligated with fluorescently labeled primers. A PCR reaction was then performed to amplify the hybridized probes. The amplified probes were fractionated on an ABI3130xl Genetic Analyzer (Applied Biosystems) and the peak patterns were evaluated using GeneMapper (Applied Biosystems).

Real-time PCR

To determine the length of each deleted genomic region, 100 ng of genomic DNA from the subjects and a normal control were subjected to quantitative PCR (Prism 7000, Applied Biosystems) using Power SYBR® Green Master Mix (Life Technologies, Carlsbad, CA, USA) and 12 sets of primers designed to amplify sequence-tagged sites on chromosome 2 (GenBank accession nos: RH46518, RH30035, RH66441, GDB603632, 1988, RH24952, RH47422, RH65573, RH26526, RH35885, RH16314, and RH92249).

Homology modeling of the PAX3 paired domain

The DNA-binding site of the paired domain of PAX3 was modeled using SWISS-MODEL [10] with the crystal structure of the PAX5 paired domain-DNA complex (PDB ID:1PDN_chain C) as the template because PAX3 and PAX5 are functionally and structurally similar [11]. The amino acid

Table I. Primer sequences for *PAX3*.

Exon 1	Forward	5′-TGTAAAACGACGGCCAGTAGAGCAGCGCGCTCCATTTG-3′
	Reverse	5′-CAGGAAACAGCTATGACCGCTCGCCGTGGCTCTCTGA-3′
Exon 2	Forward	5′-TGTAAAACGACGGCCAGTAAGAAGTGTCCAGGGCGCGT-3′
	Reverse	5′-CAGGAAACAGCTATGACCGGTCTGGGTCTGGGAGTCCG-3′
Exon 3	Forward	5′-TGTAAAACGACGGCCAGTTAAACGCTCTGCCTCCGCCT-3′
	Reverse	5′-CAGGAAACAGCTATGACCGGGATGTGTTCTGGTCTGCCC-3′
Exon 4	Forward	5′-TGTAAAACGACGGCCAGTAATGGCAACAGAGTGAGAGCTTCC-3′
	Reverse	5′-CAGGAAACAGCTATGACCAGGAGACACCCGCGAGCAGT-3′
Exon 5	Forward	5′-TGTAAAACGACGGCCAGTGGTGCCAGCACTCTAAGAACCCA-3′
	Reverse	5′-CAGGAAACAGCTATGACCGGTGATCTGACGGCAGCCAA-3′
Exon 6	Forward	5′-TGTAAAACGACGGCCAGTTGCATCCCTAGTAAAGGGCCA-3′
	Reverse	5′-CAGGAAACAGCTATGACCGGTGTCCATGGAAGACATTGGG-3′
Exon 7	Forward	5′-AACTATTATTTCATCAGTGAAATC-3′
	Reverse	5′-ATTCACTTGTATAAAATATCCACC-3′
Exon 8	Forward	5′-TGTAAAACGACGGCCAGTTGAAGCCAGTAGGAAGGGTGGA-3′
	Reverse	5′-CAGGAAACAGCTATGACCTGCAGGTTAAGAAACGCAGTTTGA-3′
Exon 9a	Forward	5′-TGTAAAACGACGGCCAGTTTGATACCGGCATGTGTGGC-3′
	Reverse	5′-CAGGAAACAGCTATGACCTGCAGTCAGATGTTATCGTCGGG-3′
Exon 9b	Forward	5′-TGTAAAACGACGGCCAGTCACAACTTTGTGTCCCTGGGATT-3′
	Reverse	5′-CAGGAAACAGCTATGACCGGGACTCCTGACCAACCACG-3′
Exon 10–11	Forward	5′-TGTAAAACGACGGCCAGTGCAAATGGAATGTTCTAGCTCCTCG-3′
	Reverse	5′-CAGGAAACAGCTATGACCGGTCAGCTCCAGGATCATATGGG-3′

sequences of the PAX3 and PAX5 paired domains were 79% homologous. The predicted PAX3 structure and the p.I59F mutation structure were superimposed on the backbone atoms of the PAX5 paired domain-DNA complex and displayed using the extensible visualization system, UCSF Chimera [12].

Results

In family 1, the proband, a 9-month-old male, was the first child of unrelated Japanese parents. Abnormal responses were found upon newborn hearing screening in the left ear, and left hearing loss was diagnosed by ABR. On physical examination, dystopia canthorum was noted, with a W-index of 2.77. The patient's mother also had dystopia canthorum, with a W-index of 2.68. She also had a history of early graying that started at age 16 years. She had not been diagnosed with WS1. According to the parents, 10 members of this family, including the proband and the mother, showed clinical features consistent with WS1 (Figure 1). ABR performed in the proband

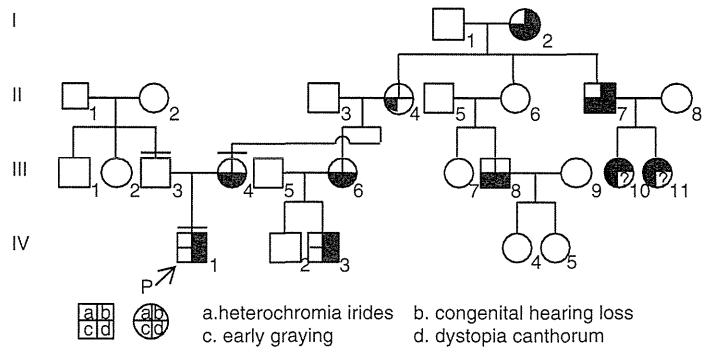

Figure 1. Pedigree of family 1. The proband is indicated by an arrow. The individuals we examined personally are indicated by a bar over the symbol. Phenotypes observed in this family are indicated symbolically as detailed below the pedigree.

revealed normal hearing in the right ear and no responses to 105 dB click stimuli in the left ear. Computed tomography (CT) of the temporal bone showed normal structures in the inner, middle, and outer ears.

Genetic analysis of *PAX3* was conducted in this family, and direct sequencing of *PAX3* revealed a heterozygous mutation, c.175A>T, in the proband and his mother. This mutation resulted in a missense mutation, p.I59F (Figure 2A). The proband's father did not harbor this mutation. p.I59F is located within exon 2 and is part of the paired domain of *PAX3*, which is a critical region for interaction between transcription factors and target DNA (Figure 2B). A multiple alignment of *PAX3* orthologs at this region demonstrated that I59 was evolutionarily conserved among various species (Figure 2C). The p.I59F mutation was not identified in any of the 184 alleles from the normal control subjects. This mutation was predicted to be 'probably damaging' according to PolyPhen-2 software.

The predicted 3D structures of the paired domain of the PAX3-DNA complex indicated that the PAX3 paired domain binds to the corresponding DNA (white double helixes) via hydrogen bonds (pink lines) at the N-terminal of α-helix1 (H1), α-helix2 (H2), and α-helix3 (H3) (indicated in blue; Figure 3A). I59 is located in the middle of H1, H2, and H3 and is surrounded by hydrophobic residues (green) protruding from H1, H2, and H3. Because the van der Waals radius of phenylalanine (Figure 3C; white arrows) is larger than that of isoleucine (Figure 3B, white arrowheads), F59 repels the surrounding hydrophobic residues by van der Waals forces and increases the distance between F59 and the surrounding hydrophobic residues, resulting in structural distortion of the DNA-binding site of PAX3. Since this site is precisely shaped for maximal binding to the corresponding DNA, this mutation is likely to reduce the binding ability of the paired domain of PAX3 and cause WSI. A mutational search found the same mutation in another Japanese family [8].

In family 2, the proband, a female aged 4 years and 4 months, was the first child of unrelated Japanese parents. Abnormal responses were found upon newborn hearing screening in the right ear, and right hearing loss was diagnosed by ABR. On physical examination, dystopia canthorum, medial eyebrow flare, and a white forelock were noted. She was admitted to hospital suffering from ketotic hypoglycemia of unknown cause when aged 4 years. Her mother presented with heterochromia iridis, dystopia canthorum, and medial eyebrow flare, and her grandmother presented with early graying that started at around 20 years of age, dystopia canthorum, and

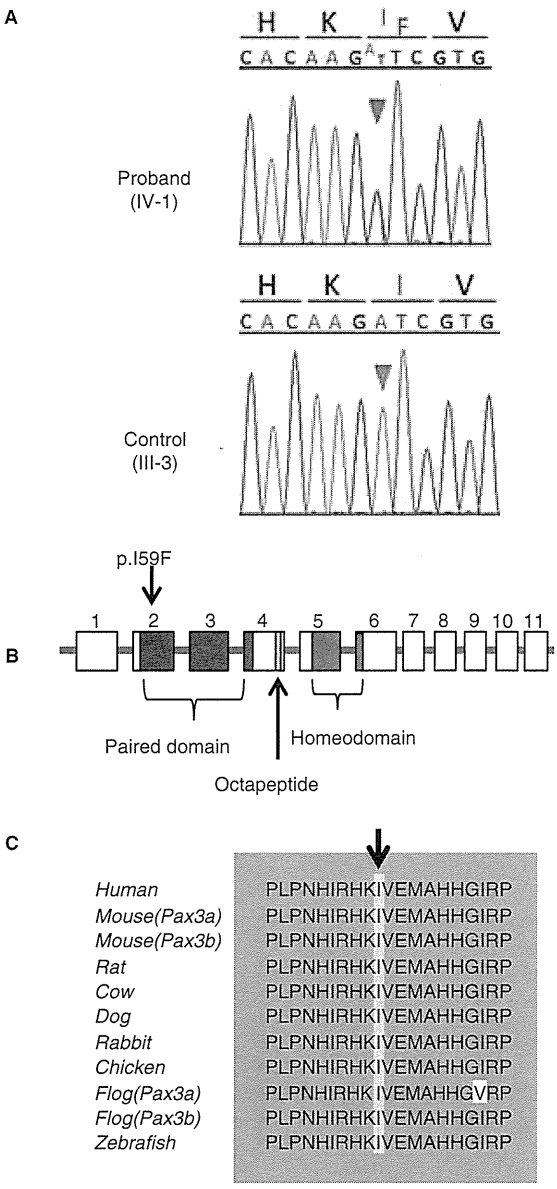

Figure 2. The p.I59F mutation of *PAX3* detected in family 1. (A) Sequence chromatogram for the proband and unaffected control. A heterozygous A to T transversion (red arrowhead) that changes codon 59 from ATC, encoding isoleucine (I), to TTC, encoding phenylalanine (F), was detected in the proband but not in the control (green arrowhead). (B) Localization of the p.I59F mutation and functional domains of PAX3. (C) A multiple alignment of PAX3 orthologs. Regions of amino acid sequence identity are shaded gray. The position of I59 is indicated by an arrow and shaded yellow.

medial eyebrow flare. According to the grandmother, the father of the grandmother also had dystopia canthorum and medial eyebrow flare. The pedigree of family 2 is shown in Figure 4. The grandmother

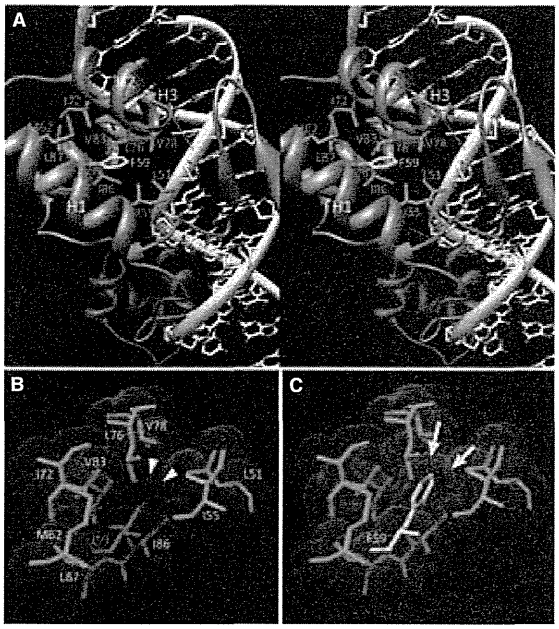

Figure 3. The predicted structure of the PAX3 paired domain-DNA complex. (A) The stereo view indicates that the mutated residue was surrounded by hydrophobic residues (green) protruding from H1, H2, and H3 of the paired domain (blue), which binds to DNA (white, sugar; blue, nitrogen; red, oxygen). The pink lines indicate hydrogen bonds. Magenta and yellow residues indicate I59 and F59, respectively. (B, C) The colored spheres indicate the van der Waals surface boundaries, the radius of the hydrophobic residues is shown in green, I59 is shown in magenta and is also indicated by arrowheads, and F59 is shown in yellow and is also indicated by arrows.

and her father had never been diagnosed with WS1. Pure tone audiometry of the proband showed severe hearing loss in the right ear and normal hearing in the left ear. The results of ABR and distortion product otoacoustic emissions in the proband were compatible with those obtained for pure tone audiometry.

Because direct sequencing of *PAX3* in the proband and her grandmother revealed no mutations, we conducted MLPA analysis to search for a large deletion of *PAX3*, and found that the copy number of all tested exons (exons 1–9) of *PAX3* was half that of the number of other chromosomal regions in both subjects (Figure 5A). In control subjects, all tested exons of *PAX3* showed the same copy number as the other chromosomal regions (Figure 5B). To determine the size of the deleted region, quantitative PCR was performed at 12 sequence-tagged sites on chromosome 2q36, which includes *PAX3*. In the proband, copy numbers at nine sites in the middle of the tested region (white arrows) were half that of those examined in normal controls, but the copy numbers at three of the sites near the 5' and 3' ends of the tested region (black arrows) were identical to those examined in normal controls (Figure 6). This result demonstrated that the chromosomal region spanning 1759–2554 kb at 2q36, which includes the whole *PAX3* gene, was deleted in one of the alleles of the proband. The same results were detected in the grandmother. A search for the deleted region revealed that this region contained between 12 and 18 genes, including *PAX3*.

Discussion

The heterozygous missense mutation, p.I59F, was identified in family 1. The pathogenicity of a novel or rare missense mutation in the causative gene is not necessarily verified even when the mutation is absent from a large number of normal controls, when the residue is evolutionary conserved among different species, or if the mutation is associated with the phenotype within a family, because an identified

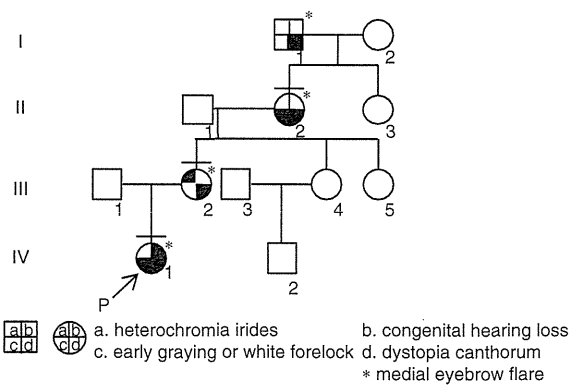

Figure 4. Pedigree of family 2. The proband is indicated by an arrow. The individuals we examined personally are indicated by a bar over the symbol. Phenotypes observed in this family are indicated symbolically, as detailed below the pedigree.

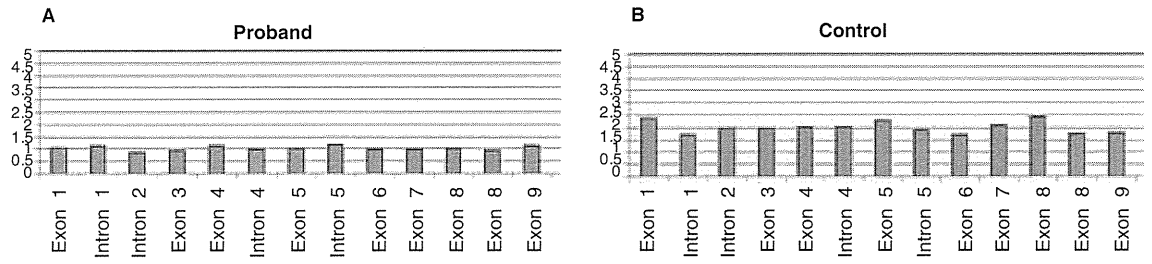

Figure 5. Results of MLPA analysis of *PAX3* in family 2. (A, B) Relative ratios of DNA quantity in each exon compared with that in the control region are shown for the proband (A) and control (B).

missense mutation may be a rare normal variant. Thus, the pathogenicity of such mutations needs to be verified by detection of the same mutation in multiple families with the same phenotype or by functional analysis. The functional consequences of a few *PAX3* mutations have been tested and reduced DNA-binding properties have been reported [13–15]. The p.I59F mutation was reported in a Japanese family [8], but functional analysis has not been conducted. We analyzed the predicted 3D structures of the paired domain of the PAX3-DNA complex and showed that this mutation was likely to distort the structure of the DNA-binding site of PAX3 and lead to functional impairment. This result substantially supports the hypothesis that the p.I59F mutation is pathogenic, although it is based on a theoretical prediction rather than functional experiments.

In family 2, the distinct phenotypes of the proband, the proband's mother, and the proband's grandmother were congenital unilateral hearing loss, heterochromia iridis, and early graying, respectively. Because of these differences, they were not aware of the hereditary nature of the symptoms. Identification of the *PAX3* mutation in the proband and the proband's grandmother led to an accurate diagnosis of WS1 and facilitated understanding of the symptoms. In this family, direct sequencing of *PAX3* did not detect any mutations, but MLPA analysis detected a large heterozygous deletion. Furthermore, quantitative PCR analysis revealed that the deleted region spanned 1759–2554 kb and included 12–18 genes. Large deletions of *PAX3* in patients with WS1 have been reported in several families [6,16–18]. To our knowledge, however, this is the largest deletion identified in patients with WS1 and has, therefore, expanded the spectrum of *PAX3* mutations. There is no reported correlation between the nature of the mutation (deleted vs truncated or missense) or

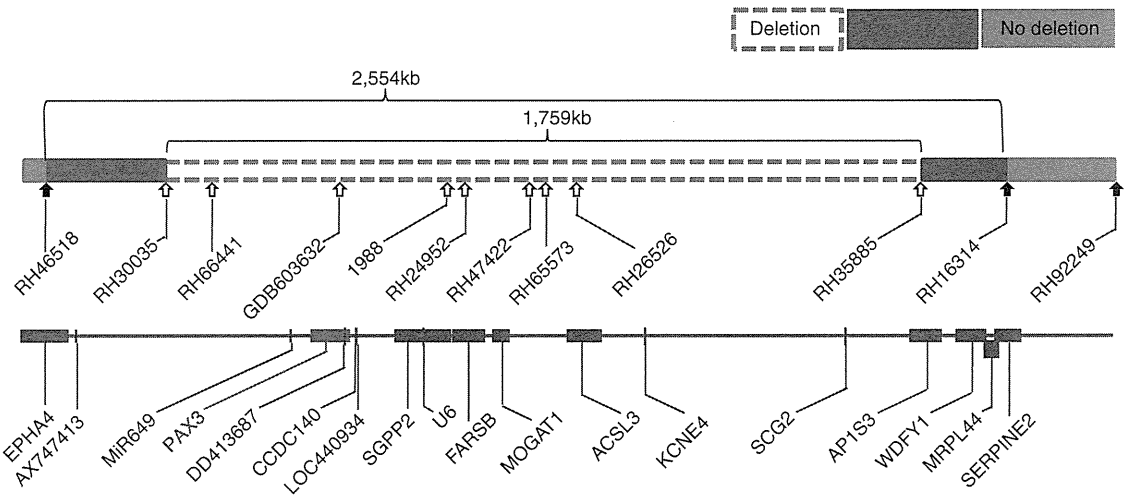

Figure 6. Genetic map showing the estimated location of the *PAX3* deletion together with the regions surrounding *PAX3*. Sites examined by quantitative PCR are indicated by arrows. Blank and white arrows indicate that the quantities of DNA at these sites are half or identical to the quantities of DNA at the corresponding sites in the control, respectively. The 5' and 3' ends of the deletion are located within the blue regions flanking the white region, designated as 'deletion,' and flanked by the green regions, designated as 'no deletion.' All genes mapped within this region, including *PAX3*, are shown in the lower map.

its location in *PAX3*, and the severity of the WS1 phenotype [19,20]. Similarly, no evidence of such a correlation was found in the data presented in this study.

In the present study, *PAX3* genetic diagnosis contributed to the accurate diagnosis of WS1. Such diagnosis could help provide genetic counseling to patients with isolated or few phenotypic symptoms, those with mild phenotypes or few first-degree relatives, or those who have yet to develop any symptoms. In addition, analysis of the predicted 3D structure of PAX3 facilitated the verification of pathogenicity of a missense mutation, and MLPA analysis increased the sensitivity of genetic diagnosis of WS1.

Acknowledgments

We thank the families that participated in this study. This study was supported by a Grant-in-Aid for Clinical Research from the National Hospital Organization, and by a Health and Labour Sciences Research Grants for Research on Rare and Intractable Diseases from the Ministry of Health, Labour and Welfare of Japan.

Declaration of interest: The authors report no conflicts of interest. The authors alone are responsible for the content and writing of the paper.

References

[1] Read AP, Newton VE. Waardenburg syndrome. J Med Genet 1997;34:656–65.
[2] Farrer LA, Grundfast KM, Amos J, Arnos KS, Asher JH Jr, Beighton P, et al. Waardenburg syndrome (WS) type I is caused by defects at multiple loci, one of which is near ALPP on chromosome 2: first report of the WS consortium. Am J Hum Genet 1992;50:902–13.
[3] Liu XZ, Newton VE, Read AP. Waardenburg syndrome type II: phenotypic findings and diagnostic criteria. Am J Med Genet 1995;55:95–100.
[4] Pardono E, van Bever Y, van den Ende J, Havrenne PC, Iughetti P, Maestrelli SR, et al. Waardenburg syndrome: clinical differentiation between types I and II. Am J Med Genet A 2003;117A:223–35.
[5] Pingault V, Ente D, Dastot-Le Moal F, Goossens M, Marlin S, Bondurand N. Review and update of mutations causing Waardenburg syndrome. Hum Mutat 2010;31: 391–406.
[6] Milunsky JM, Maher TA, Ito M, Milunsky A. The value of MLPA in Waardenburg syndrome. Genet Test 2007;11:179–82.
[7] Ishikiriyama S, Tonoki H, Shibuya Y, Chin S, Harada N, Abe K, et al. Waardenburg syndrome type I in a child with de novo inversion (2)(q35q37.3). Am J Med Genet 1989;33: 505–7.
[8] Soejima H, Fujimoto M, Tsukamoto K, Matsumoto N, Yoshiura KI, Fukushima Y, et al. Three novel PAX3 mutations observed in patients with Waardenburg syndrome type 1. Hum Mutat 1997;9:177–80.
[9] Kashima T, Akiyama H, Kishi S. Asymmetric severity of diabetic retinopathy in Waardenburg syndrome. Clin Ophthalmol 2011;5:1717–20.
[10] Kiefer F, Arnold K, Kunzli M, Bordoli L, Schwede T. The SWISS-MODEL Repository and associated resources. Nucleic Acids Res 2009;37:D387–92.
[11] Xu W, Rould MA, Jun S, Desplan C, Pabo CO. Crystal structure of a paired domain-DNA complex at 2. 5 A resolution reveals structural basis for Pax developmental mutations. Cell 1995;80:639–50.
[12] Pettersen EF, Goddard TD, Huang CC, Couch GS, Greenblatt DM, Meng EC, et al. UCSF Chimera – a visualization system for exploratory research and analysis. J Comput Chem 2004;25:1605–12.
[13] Chalepakis G, Goulding M, Read A, Strachan T, Gruss P. Molecular basis of splotch and Waardenburg Pax-3-mutations. Proc Natl Acad Sci USA 1994;91:3685–9.
[14] Corry GN, Underhill DA. Pax3 target gene recognition occurs through distinct modes that are differentially affected by disease-associated mutations. Pigment Cell Res 2005;18: 427–38.
[15] Fortin AS, Underhill DA, Gros P. Reciprocal effect of Waardenburg syndrome mutations on DNA binding by the Pax-3 paired domain and homeodomain. Hum Mol Genet 1997;6:1781–90.
[16] Baldwin CT, Lipsky NR, Hoth CF, Cohen T, Mamuya W, Milunsky A. Mutations in PAX3 associated with Waardenburg syndrome type I. Hum Mutat 1994;3:205–11.
[17] Tassabehji M, Newton VE, Leverton K, Turnbull K, Seemanova E, Kunze J, et al. PAX3 gene structure and mutations: close analogies between Waardenburg syndrome and the Splotch mouse. Hum Mol Genet 1994;3: 1069–74.
[18] Wang J, Li S, Xiao X, Wang P, Guo X, Zhang Q. PAX3 mutations and clinical characteristics in Chinese patients with Waardenburg syndrome type 1. Mol Vis 2010;16:1146–53.
[19] Baldwin CT, Hoth CF, Macina RA, Milunsky A. Mutations in PAX3 that cause Waardenburg syndrome type I: ten new mutations and review of the literature. Am J Med Genet 1995;58:115–22.
[20] Tassabehji M, Newton VE, Liu XZ, Brady A, Donnai D, Krajewska-Walasek M, et al. The mutational spectrum in Waardenburg syndrome. Hum Mol Genet 1995;4: 2131–7.

CHAPTER 9

Cellular Properties of Mesenchymal Cells Derived from the Decidua of Human Term Placenta and Their Applications in Regenerative Medicine

Daisuke Kanematsu[1] and Yonehiro Kanemura[1,2,*]

Introduction

Regenerative medicine offers promising new methods for treating various intractable diseases and damaged organs, by using advanced techniques and human stem cells processed *ex vivo*. Preclinical and clinical studies using stem cells from various somatic tissues have reported encouraging results

[1]Division of Regenerative Medicine, Institute for Clinical Research, Osaka National Hospital, National Hospital Organization, 2-1-14 Hoenzaka, Chuo-ku, Osaka 540-0006, Japan.
[2]Department of Neurosurgery, Osaka National Hospital, National Hospital Organization, 2-1-14 Hoenzaka, Chuo-ku, Osaka 540-0006, Japan.
*Corresponding author: kanemura@onh.go.jp

(Goldman 2005, Koch et al. 2009, Phinney and Prockop 2007), and the first clinical trial using human embryonic stem cell (hESC)-derived cells to treat spinal cord injuries is underway (Bretzner et al. 2011).

The choice of human stem cells for use in clinical applications is critical, requiring careful consideration of the cell's progenitor type and tissue of origin (Goldman 2005, Koch et al. 2009, Phinney and Prockop 2007). Patient-derived autologous somatic stem cells are presently the most desirable choice for regenerative treatment, for reasons of both safety and ethics (Goldman 2005, Koch et al. 2009, Phinney and Prockop 2007). This ideal cell therapy may become a reality with the use of recently developed reprogramming techniques for generating human-induced pluripotent stem cells (hiPSCs) (Takahashi et al. 2007). The transplantation of allogeneic human fetus-derived stem cells (Goldman 2005, Koch et al. 2009) or hESCs (Thomson et al. 1998) is also promising, and the use of these cells will become more feasible as cell banking systems are established.

Human stem cells for clinical use must be prepared and stored following strict aseptic processing procedures in order to prevent contamination with microbiological and hazardous materials. These steps involve difficult and time-consuming techniques. The cell processing and banking systems necessary to generate and maintain various human stem cells for clinical use are still being developed.

This chapter describes the cellular properties of mesenchyme (stem) cells derived from fetal adnexal tissues, and discusses their use in regenerative medicine.

The Fetal Adnexa

The fetal adnexal tissues contain extra-embryonic cells and include the placenta, which connects the developing fetus to the uterine wall, the fetal membrane, which wraps the fetus and amniotic fluid within the uterus, and the umbilical cord, which contains umbilical cord blood cells (UCBs) and connects the fetus and the mother (Fig. 9.1A) (Parolini et al. 2008, Ilancheran et al. 2009). Histologically, the fetal membrane and the placenta are composed of three layers—the amnion, chorion, and decidua (Fig. 9.1A and B).

The amnion, chorion, and umbilical cord (including the UCBs) are all of fetal origin, but the decidua is maternal (In 't Anker et al. 2004). Maternal and fetal tissues intertwine at the placental barrier (In 't Anker et al. 2004, Wulf et al. 2004, Parolini et al. 2008). The fetal adnexa connect the developing fetal tissues to the uterine wall, encase the amniotic fluid in which the fetus is suspended, supply the fetus with maternal nutrients, allow fetal waste to be disposed via the maternal kidneys, and contribute to fetal-maternal immune tolerance (Parolini et al. 2008, Ilancheran et al. 2009).

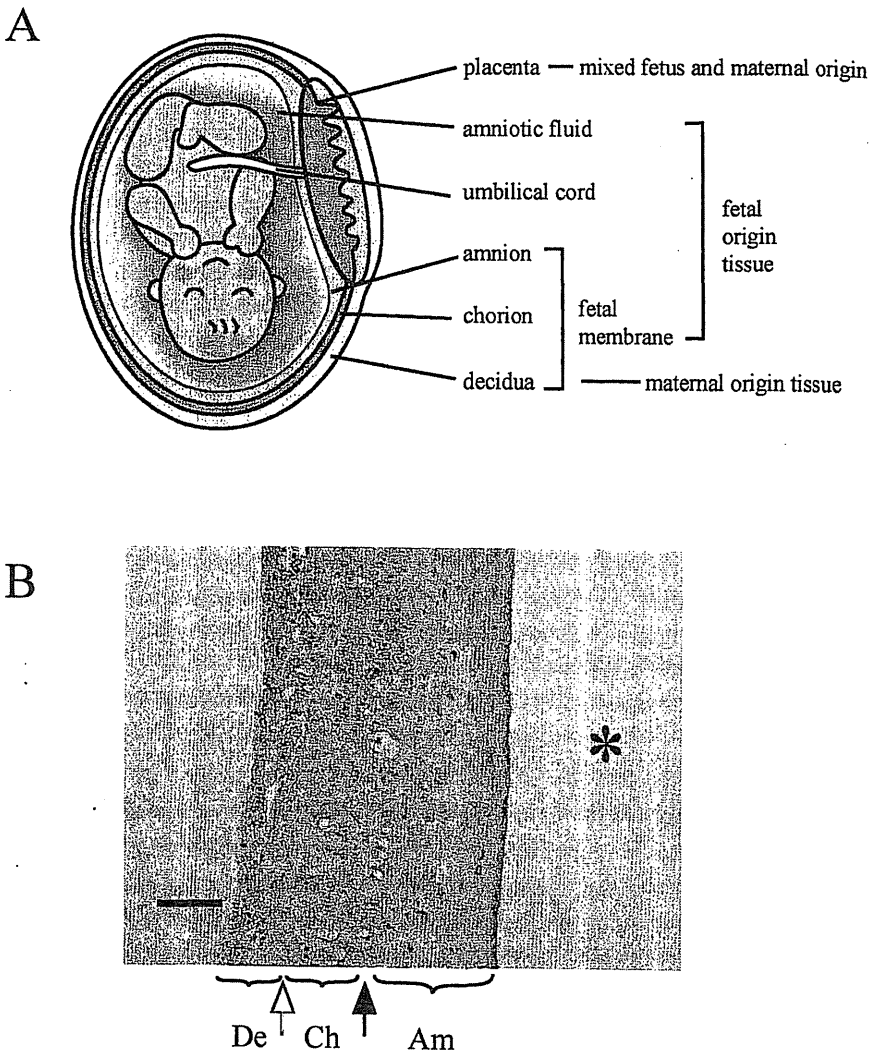

Figure 9.1 Structures and Content of Fetal Adnexa Tissue. (A) Schematic of the fetus and fetal adnexal tissues. (B) Structure of human fetal membranes with the decidua vera: hematoxylin and eosin staining. The chorionic tissue is shown between the closed and open arrowheads. Am: amnion; Ch: chorionic tissue; De: decidua tissue; * indicates fetal side. Scale bar =100 μm.

Mesenchymal Stem Cells (MSCs) Derived from Fetal Adnexa

MSCs are a heterogeneous subset of stromal stem cells with fibroblast-like morphology. MSCs *in vitro* proliferate as plastic-adherent cells, form colonies, and differentiate into bone, cartilage, and fat cells (Caplan 1991, Horwitz et

al. 2005, Dominici et al. 2006, Uccelli et al. 2008). MSCs are typically derived from bone marrow non-hematopoietic mononuclear cells (BM-MSCs), but they can be isolated from many fetal and adult tissues (Parolini et al. 2008, Koide et al. 2007, Ilancheran et al. 2009, Marcus and Woodbury 2008, Caplan 1991, Pittenger et al. 1999, Dominici et al. 2006, Uccelli et al. 2008). Several studies have shown that fibroblast-like adherent cells isolated from various components of the fetal adnexa are phenotypically similar to MSCs. MSCs have been isolated specifically from the amnion (In 't Anker et al. 2004, Bailo et al. 2004, Portmann-Lanz et al. 2006, Alviano et al. 2007, Ilancheran et al. 2007), chorion (Bailo et al. 2004, Portmann-Lanz et al. 2006), chorionic villi (Igura et al. 2004, Zhang et al. 2006), villous stroma of the para-umbilical area (Wulf et al. 2004), decidua basalis (Huang et al. 2009), and the internal portion of the placental lobules (Fukuchi et al. 2004). Others have also been isolated from mixed placental tissues from two or three layers (Zhang et al. 2004, Yen et al. 2005, Li et al. 2005, Miao et al. 2006, Battula et al. 2007, Barlow et al. 2008). Thus, the fetal adnexa merit attention as a new source of human MSCs (Tables 9.1, 9.2) (Fukuchi et al. 2004, Igura et al. 2004, Zhang et al. 2004, In 't Anker et al. 2004, Wulf et al. 2004, Bailo et al. 2004, Yen et al. 2005, Li et al. 2005, Portmann-Lanz et al. 2006, Miao et al. 2006, Battula et al. 2007, Alviano et al. 2007, Soncini et al. 2007, Ilancheran et al. 2007, Barlow et al. 2008).

It is important to determine the origins of MSCs derived from fetal adnexa, and studies have clearly defined the origins of MSCs as maternal (In 't Anker et al. 2004, Wulf et al. 2004, Soncini et al. 2007, Barlow et al. 2008) or fetal (Fukuchi et al. 2004, Igura et al. 2004, Zhang et al. 2006). Other studies, relying on a less thorough analysis, have concluded that all MSCs isolated from placental tissues are of fetal origin. Therefore, both the precise origin and detailed biological properties of the MSCs derived from various human fetal adnexal tissues remain to be determined.

Decidua-Derived Mesenchymal Cells (DMCs)

Adherent decidua-derived mesenchymal cells (DMCs) were recently isolated from human term decidua vera, and their unique properties reported in detail (Nagase et al. 2009, Kanemura 2010, Kanematsu et al. 2011). The DMCs were prepared by washing the fetal membrane (Fig. 9.1A and B) repeatedly with phosphate buffered saline (PBS), gently separating the amnion (Fig. 9.1B, Am) from the area above the chorion (Fig. 9.1B, closed arrow) and manually (macroscopically) scraping the decidua vera (Fig. 9.1B, De) from the chorionic membrane (Fig. 9.1B, Ch, open arrow) to obtain pure decidual tissue samples without chorionic contamination. The decidual tissue (Fig. 9.1B, De) was dissected into small pieces; enzymatically dissociated using

Table 9.1 The *in vitro* multipotency of mesenchymal stem cells derived from fetal adnexa tissue.

References	Chondrogenesys	Adipogenesys	Osteogenesys
amnion tissue origin			
Alviano et al. 2007	+	+	+
Ilancheran et al. 2007	/	+	+
In't Anker et al. 2004	/	+	+
Portmann-Lanz et al. 2006 (mesenchymal cells)	+	+	+
Soncini et al. 2007	+	+	+
Stadler et al. 2008 (epithelial cells)	/	/	+
Stadler et al. 2008 (mesenchymal cells)	/	+	+
Sudo et al. 2007	+	-	+
chorion (villous) tissue origin			
Igura et al. 2004	+	+	+
Portmann-Lanz et al. 2006 (chorion mesenchymal cells)	+	+	+
Portmann-Lanz et al. 2006 (chorionic villous storomal cells)	+	+	+
Soncini et al. 2007	+	+	+
Wulf et al. 2004	+	+	+
Zhang et al. 2006	+	/	/
decidua tissue origin			
Huang et al. 2009 (decidua basalis)	+	+	+
In't Anker et al. 2004 (decidua basalis)	/	+	+
In't Anker et al. 2004 (decidua parietalis)	/	+	+
Kanematsu et al. 2011 (decidua vera)	+	±	-
placenta tissue origin			
Battula et al. 2007	/	+	+
Fukuchi et al. 2004	/	+	+
Li et al. 2005	+	+	+
Yen et al. 2005	/	+	+
Zhang et al. 2004	+	+	+
other tissue origin			
Barlow et al. 2008 (amnion, chorion, and decidua mix)	+	±	+
In't Anker et al. 2004 (amniotic fluid)	/	+	+

+: positive, -: negative, ±: low positive, /: not mentioned.

a mixture of collagenase, dispase and DNase I; and filtered through a nylon mesh. Single-cell suspensions were propagated in cell-culture dishes using DMEM/F-12 (1:1)-based culture medium supplemented with 10 percent fetal bovine serum (FBS) at 37°C in 5 percent CO_2. After several days, some DMCs had adhered to the bottom of the vessel. The primary DMCs generally reached confluence after several weeks of culture with replacement of the culture medium two times per week. The confluent cells were easily passaged by standard procedures using trypsin–EDTA (Kanematsu et al. 2011).

Table 9.2 Patterns of cell surface markers of mesenchymal stem cells derived from fetal adnexa tissue.

	commonly used positive markers										commonly used negative markers							
References	CD13	CD29	CD44	CD54	CD73 (SH3-4)	CD90	CD105 (SH2)	CD166	HLA-ABC (MHC-I)	other positive markers	CD3	CD14	CD31	CD34	CD45	CD133	HLA-DR (MHC-II)	other negative markers
amnion tissue origin																		
Alviano et al. 2007	/	+	+	/	+	/	+	+	/		/	-	/	-	-	/	/	
Bailo et al. 2004	/	+	+	+	+	+	+	/	/		-	-	/	-	-	/	/	
Hancheran et al. 2007	/	/	/	/	/	/	/	/	-		/	/	/	/	/	/	-	
In't Anker et al. 2004	/	/	/	/	+	+	+	+	+	CD49e	/	/	-	-	-	/	-	CD49d, CD123
Portmann-Lanz et al. 2006 (amnion epithelial cells)	+	+	+	/	+	+	+	+	+		/	-	/	-	-	/	-	CD49e
Portmann-Lanz et al. 2006 (amnion mesenchymal cells)	+	+	+	/	+	+	+	+	+	CD49e	/	-	/	-	-	/	-	
Soncini et al. 2007	+	+	+	+	+	/	+	+	/		-	-	-	-	-	/	/	
Stadler et al. 2008	+	+	+	+	+	+	+	+	/	CD49e, CD49e, SSEA-4, Ki67	/	-	/	-	-	/	/	CD49d, TRA-1-60,TRA-1-81
Sudo et al. 2007	/	+	+	/	/	+	+	+	/		/	-	-	-	-	/	/	
chorion (villous) tissue origin																		
Bailo et al. 2004	/	+	+	+	+	+	+	/	/		-	-	/	-	-	/	/	
Igura et al. 2004	+	/	+	/	+	+	+	/	+		/	/	-	-	-	/	-	
Portmann-Lanz et al. 2006 (chorion mesenchymal cells)	+	+	+	/	+	+	+	+	+	CD49e	/	-	/	-	-	/	-	
Portmann-Lanz et al. 2006 (chorionic villous stromal cells)	+	+	+	/	+	+	+	+	+	CD49e	/	-	/	-	-	/	-	
Soncini et al. 2007	+	+	+	+	+	/	+	+	/		-	-	-	-	-	/	/	
Wulf et al. 2004	+	+	/	/	+	/	-	/	/	CD9	/	-	/	-	-	/	/	CD117, Stro-1, AS02
Zhang et al. 2006	/	+	+	/	+	+	+	/	+		/	/	-	-	-	-	-	Tie2
decidua tissue origin																		
Huang et al. 2009	/	+	+	/	/	/	+	+	+	CD9, SSEA-1,SSEA-3,SSEA-4, TRA-1-60, TRA-1-81, OCT4	/	/	/	-	/	/	-	CD40L
In't Anker et al. 2004 (decidua basalis)	/	/	/	/	+	+	+	+	+	CD49e	/	/	-	-	-	/	-	CD49d, CD123
In't Anker et al. 2004 (decidua parietalis)	/	/	/	/	+	+	+	+	+	CD49e	/	/	-	-	-	/	-	CD49d, CD123
Kanematsu et al. 2011	+	+	+	/	+	+	+	+	+	anti-fibroblast, SSEA-4	/	-	/	-	+	/	-	CD19, CD271
placenta tissue origin																		
Battula et al. 2007	/	/	/	/	/	/	+	/	/	CD318	/	/	/	/	/	/	/	SSEA-4, FZD9, FZD10, W8B2B10
Fukuchi et al. 2004	/	+	+	+	/	/	/	/	/		/	/	-	/	+	/	/	AC133
Li et al. 2005	/	+	+	/	+	/	+	+	+		/	/	-	-	-	/	-	
Miao et al. 2006	/	+	+	/	/	/	+	/	/		/	/	/	-	-	/	-	
Yen et al. 2005	/	+	+	/	+	+	+	+	+	CD9, SSEA-4, TRA-1-60, TRA-1-81	/	-	/	-	-	/	-	AC133/2, CD117, CD40L, CD80, CD86, HLA-G, cytokeratin7
Zhang et al. 2004	/	+	+	/	+	/	+	+	+		/	-	/	-	-	/	-	
other tissue origin																		
Barlow et al. 2008 (amnion, chorion, and decidua mixture)	/	+	+	/	+	+	+	+	+		/	/	/	-	-	/	-	
In't Anker et al. 2004 (amniotic fluid)	/	/	/	/	+	+	+	+	+	CD49e	/	/	-	-	-	/	-	CD49d, CD123

+: positive, -: negative, ±: low positive, /: not mentioned.

The DMC Phenotype in vitro

Morphology and Cytoskeletal Components

DMCs have a fibroblast-like cell morphology (Fig. 9.2A). Consistent with their morphology, Phalloidin staining shows their F-actin cytoskeleton extending throughout the cytoplasm in a strong fibrillar pattern

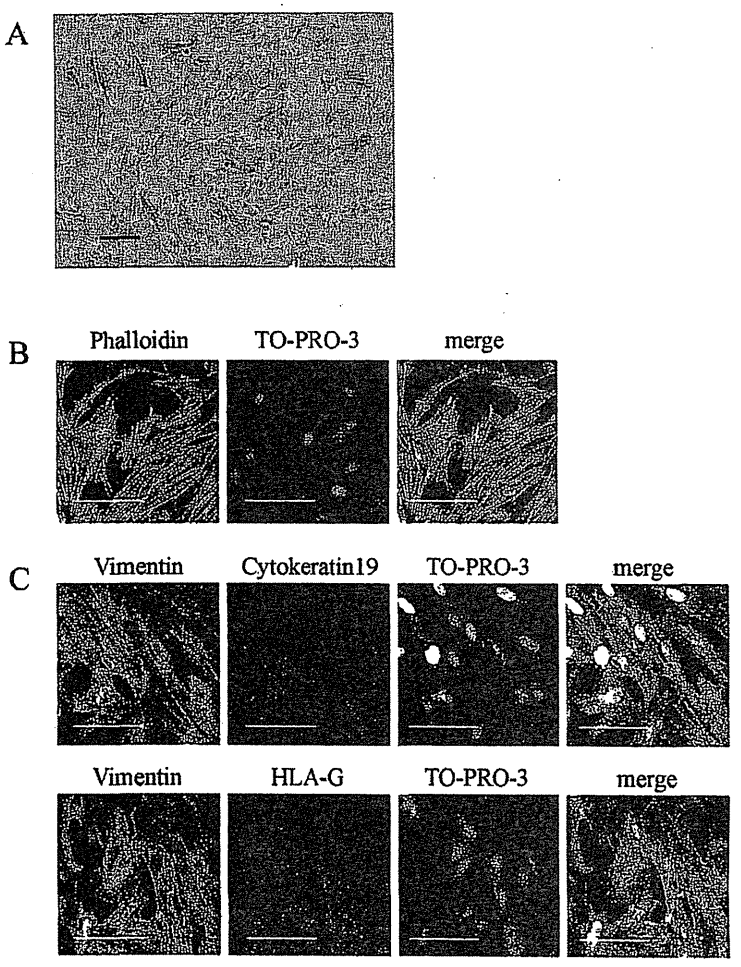

Figure 9.2 The *in vitro* Phenotype of DMCs.

(A) Phase contrast image of DMCs (4 passages, 40 DIV). Scale bar = 100 µm.
(B) Phalloidin-stained fluorescent images of the DMC F-actin cytoskeleton (3 passages, 37 DIV). Nuclei were counterstained with TO-PRO-3. Scale bar = 100 µm.
(C) Fluorescent immunocytochemical analysis with vimentin and cytokeratin 19 or HLA-G on DMCs (5 passages, 45 DIV). Nuclei were counterstained with TO-PRO-3. Scale bar = 100 µm.

(Fig. 9.2B). In addition, DMCs express vimentin but not cytokeratin 19 (CK19) or HLA-G (vimentin+/CK19-/HLA-G-cells) (Fig. 2C), suggesting a mesenchymal lineage (Kanematsu et al. 2011).

Growth Properties

DMCs displayed reproducibly good growth properties, growing exponentially for almost 90 dy *in vitro* (DIV) with proliferation gradually diminishing after 120 DIV (Fig. 9.3).

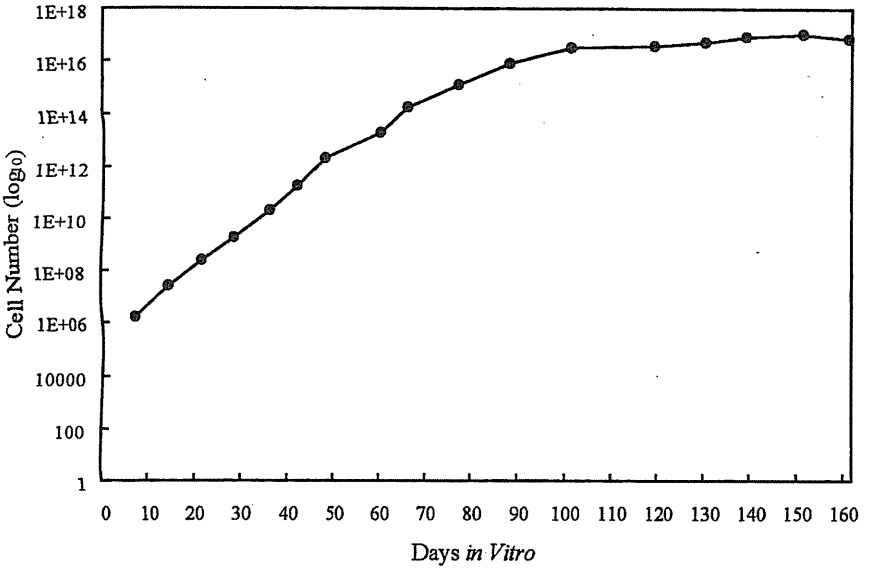

Figure 9.3 Representative DMC Growth Rates. DMCs maintained a high proliferation rate through an estimated 34.4 ± 4.5 (mean ± S.D.) population doublings (Kanematsu et al. 2011). In colony-forming unit-fibroblast (CFU-F) assays of BM-MSC lines and of DMCs at the second passage, DMCs consistently formed very dense, compact colonies; BM-MSC colonies were loose and sparsely populated by comparison, illustrating that BM-MSCs and DMCs differ in cell growth properties.

Cell-Surface Antigen Expression

Flow cytometry analysis of surface antigens showed that more than 90 percent of DMCs had high levels of CD13, CD29, CD44, CD73, CD90, CD166, and HLA-ABC antigens, and that more than 60 percent also expressed CD105 (Kanematsu et al. 2011). In contrast, less than 3 percent of DMCs expressed CD14, CD19, CD34 or HLA-DR antigens (Kanematsu et al. 2011). Some cells expressed SSEA-4 or CD45, and over 50 percent of these also expressed anti-fibroblast antigen. However, only a very minor